International Journal of Engineering

Journal Homepage: www.ije.ir

A Macro-model for Nonlinear Analysis of 3D Reinforced Concrete Shear Walls

M. Heydari, F. Behnamfar*, H. Zibasokhan

Department of Civil Engineering, Isfahan University of Technology, Esfahan, Iran

PAPER INFO

Paper history:
Received 09 May 2016
Received in revised form 13 September 2017
Accepted 12 October 2017

Keywords:
Micro Model
Meso Model
Macro Model
Nonlinear Analysis
3D RC Shear Wall

ABSTRACT

In this research about 450 cases of 3D shear walls are considered with different shapes and heights. L, T and H-shape walls are studied. They are nonlinearly analyzed in Abaqus using a micro-model, i.e. the finite element modeling and analysis. A meso-modeling approach using fiber elements is also examined in Opensees. It is shown that the meso-model is both accurate enough and much faster than the micro modeling approach. To go further, a macro-model is developed in bending in which the nonlinear behavior is assumed to be concentrated at the base of the wall using a rotational spring. The axial force, shape of the cross section, percentage of the longitudinal reinforcement and the aspect ratio of the wall are recognized to be the main parameters defining characteristics of the rotational spring. Using regression, semi-analytical formulas are suggested for rapid determination of the moment-rotation curve of the rotational spring. Comparison with micro-model and available experimental results confirm the good accuracy of the developed macro-model.

doi: *10.5829/ije.2018.31.02b.05*

1. INTRODUCTION

The nonlinear modeling and analysis of planar RC shear walls are now well documented to the extent that documents like ASCE41-13 [1] give comprehensive details of their modeling for engineering purposes. On the other hand, in many cases because of unavoidable presence of stiff cores within the building plans, like the perimeter walls of stairways or elevators, designers tend to adopt shear walls with 3D shapes. The 3D configurations include L, T and H-shape walls. Number of research works on the nonlinear behavior of 3D shear walls is relatively small.

Regarding experimental works, Zhang and Li [2] cyclically tested six L-shape shear walls with intermediate aspect ratios. Zhang and Lu [3] experimentally compared the nonlinear behavior of rectangular and L-shape walls. The ductility capacity of T-shape walls was investigated by Taylor et al. [4], Thomsen and Wallace [5], and Chen et al. [6]. A more extensive damage was observed at the web.

As for the numerical studies, micro, meso and macro-modeling procedures have been adopted by different researchers. In the micro modeling, use is made of the finite element method to perform a detailed study on distribution of response within the body of wall. Examples of such studies on shear walls are those of references [7-11]. As the most rigorous approach, a micro-model takes much time and effort to be constructed and analyzed. Thus, it is only suitable for small specimens and a local behavior study. The meso-model consists of one-dimensional (1D) elements along height of walls called fibers. Using these elements, behavior of the wall is controlled at several pre-defined sections. At these sections, an appropriate kinematic rule like the Euler–Bernoulli or Timoshenko beam rule is enforced. The section is decomposed to steel and concrete fibers with each fiber obeying a 1D nonlinear (or hysteretic) stress-strain relation.

The macro-modeling is the largest scale model among the numerical procedures. Such models are suitable for analysis of general behavior of structural systems. Therefore, as opposed to time consuming micro and meso-modeling that process the local behavior, the macro models are much faster and more practical. The most important feature of these models is that integration of stresses at the sections is no more required. Because of their computational efficiency,

*Corresponding Author's Email: farhad@cc.iut.ac.ir (F. Behnamfar)

Please cite this article as: M. Heydari, F. Behnamfar, H. Zibasokhan, A Macro-model for Nonlinear Analysis of 3D Reinforced Concrete Shear Walls, International Journal of Engineering (IJE), IJE TRANSACTIONS B: Applications Vol. 31, No. 2, (February 2018) 220-227

several macro models have been developed in the past, like the equivalent frame model, the concentrated plasticity model [12, 13], the distributed plasticity model [14], and the multi spring model (such as the Three Vertical Lines Element Model, TVLEM [15], and the four-spring model [16, 17]).

As observed, studies on the 3D RC shear walls are still rare regarding both experimental and analytical aspects. With this incentive, in this paper a tri-linear macro model is presented for bending of 3D shear walls being L, T and H-shape in cross section.

2. THE MICRO AND MESO MODELS

2. 1. The Micro Model Micro-modeling of the RC shear walls in this study is performed using the nonlinear finite element analysis with Abaqus [18].

2. 1. 1. The Finite Elements Utilized Generally, the concrete medium is modeled with solid 3D elements. For the rebars, use is made of 1D elements. The longitudinal and transverse reinforcements are modeled using T3D2 that is a 1D element with three translational degrees of freedom at each of its two end nodes. 20-node C3D20 element with three translational degrees of freedom at each node is used for concrete modeling.

2. 1. 2. The Material Properties

Concrete

For definition of a nonlinear concrete material, the following properties should be described: modulus of elasticity, ultimate compressive strength, Poisson's ratio, ultimate tensile stress, the stress-strain relation. The cracking strain of concrete is taken to be 0.002.

For the stress-strain relation of concrete in compression, use is made of the modified Hognestaad equation. For the parametric studies of this research, $f'_c=24MPa$ and the ultimate compressive strain of plain concrete is assumed to be 0.0038 [19].

The concrete material to be used within Abaqus is of the Concrete Damaged Plasticity type. In such a brittle material type, cracking in tension and crushing in compression are included, using an equivalent plastic strain in tension and compression. The dilation angle and the Poisson's ratio are among the important material properties in such a material type. These are taken as 36 degrees and 0.2, respectively. In loading and unloading cycles of concrete in hysteretic behavior, because of cracking, the initial stiffness in tension and compression are reduced by d_t and d_c factors, respectively, varied between 1 and 0.

Steel

The material selected for the steel rebars in this study is of AIII type. The modulus of elasticity, the yield strength, and the ultimate strength are 2×10^5, 400 and 600 MPa, respectively. The yield strain, strain at the end of the plastic zone, strain at the ultimate strength, and the final strain are taken to be 0.002, 0.01, 0.07 and 0.14 [20].

2. 2. The Meso Model As mentioned, the meso modeling is performed using fibers in this study, within Opensees [21]. This study focuses on flexural walls, i.e. the walls governed by bending. Fiber modeling of such walls is accomplished as follows.

2. 2. 1. Modeling With Fibers Each fiber is a 1D element following the Bernoulli rule for beams in bending of the whole section. Rebars of the wall section are defined as single fibers. The 3D wall's section is divided into rectangles. Then each rectangle is discretized with a number of fibers. The shear behavior is taken to be elastic. The lateral force-displacement behavior of wall is assumed to be nonlinear with a distributed plasticity along the fiber length.

2. 2. 2. Material Properties

Concrete

Among the available concrete material types in Opensees, the Concrete02 material is selected [21]. This is a material appropriate for modeling of uniaxial behavior of concrete with linear and nonlinear behaviors in tension and compression.

Steel

The reinforcing steel material of Opensees [21] is used. This material type includes the strain hardening, buckling and low cycle fatigue in cyclic behavior.

2. 3. Numerical Comparison Accuracy of modeling with fibers is compared in this section with the FEM. Since the meso (fiber) analysis is much faster than of the micro models, the meso models are clearly the only practical alternative for parametric analysis of a large number of walls, as of this study.

First, accuracy of the meso models has to be established. For this purpose, an experimental wall with available details of study is selected.

2. 3. 1. The Experimental Shear Wall of Adebar et al. Adebar et al. [22] performed a cyclic testing on a 12 m tall wall as a 1:4 scale of an actual wall. A constant vertical load of about 10% of the net axial strength of the concrete of the wall was applied to the wall during the lateral cyclic testing of wall. The compressive strength of concrete was 49 MPa and the yield and ultimate stresses of steel were 450 and 650 MPa, respectively.

The same wall is modeled using the FEM and the fibers as described in the previous sections. The lateral behavior of the wall in the test is compared with those

obtained using the micro and meso models in Figure 1. A very good similarity is observed between the data sets.

3. THE MACRO MODEL OF THE 3D WALLS

3. 1. General As mentioned in Sec. 1, a macro model of a shear wall contains a wall being linear throughout and a nonlinear rotational spring being concentrated at the base of wall to represent the moment-rotation behavior. Such a model is a simple and fast computational tool for calculation of the general lateral behavior of such a wall with much less effort compared to the micro and meso models discussed. Of course, such a tool cannot be used for calculation of local behavior. In this section, first the macro model of this study, is developed for nonlinear static analysis. Since good accuracy and computation speed of the fiber analysis were established in the previous section, and regarding the large number of shear walls, accuracy of the developed macro model will be shown in comparison with the meso model.

3. 2. The Moment-Rotation Path If a cantilever wall is subjected to an increasing lateral load, the lateral behavior is linear only up to the onset of tensile cracks at the lower end of wall. Increasing the lateral load causes the farthest longitudinal rebars of the wall section to begin yielding and the maximum compressive stress of concrete at the opposite points becomes larger up to the point when crushing of concrete and failure of section happens. Slope of the force-displacement curve decreases suddenly at cracking of concrete and becomes almost zero when the main longitudinal reinforcement of wall yields in tension. The inelastic deformations extend from base of the wall upwards. With the above description in mind, and to retain simplicity as well as accuracy, in this study a tri-linear path is proposed for the moment-rotation behavior at the base of a 3D shear wall. This is shown schematically in Figure 2.

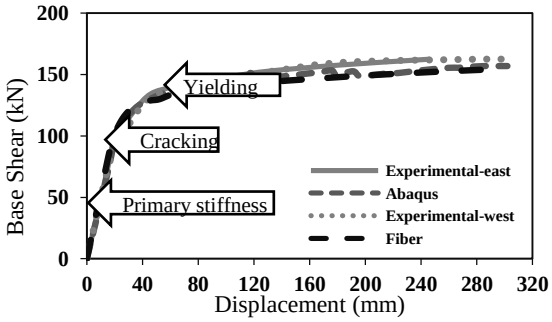

Figure 1. The lateral behavior of the wall of Adebar et al. [22] in the test and in the analysis of this study

Here, it is perceived that the relative rotation at the wall base is zero before concrete cracking at the cracking moment, M_{cr}. After that, the behavior is nonlinear up to the maximum moment M_2 where (almost) all of the tensile longitudinal rebars have yielded. A simple path (shown with solid lines) substituting the exact behavior (shown with a dashed curve) consists of one vertical and one horizontal segment and an inclined line in between. The inclined line begins at an equivalent yield moment M_1 and continues with a constant slope K_{sp}. Construction of the macro model of Figure 2 needs knowing only three parameters M_1, M_2, and K_{sp}. Thus, the simplicity is retained. Accuracy of the model goes to as how M_1 and K_{sp} are calculated. Contrary to M_2, the ultimate moment capacity, M_1 and K_{sp} are not direct physical parameters; instead, they are "tuning" parameters to be determined in a way to gain enough accuracy in moment-rotation behavior prediction. A large number of 3D walls will be analyzed using the meso model for regression analysis and derivation of general semi-analytical formulas for the mentioned parameters.

3. 3. Calculation of the Section Properties

3. 3. 1. Flexural Rigidity The flexural rigidity of the wall is taken to be E_cA_g throughout with E_c being the modulus of elasticity of concrete and A_g the gross concrete section area (without excluding the rebars).

3. 3. 2. The Ultimate Moment, M_2 The ultimate moment M_2 is simply calculated assuming a linear strain variation over the cross section of wall and well known procedures of RC design. The calculation steps of M_2 is shown as an example for H-shape walls in Figure 3.

3. 3. 3. Stiffness of The Rotational Spring, K_{sp} The post-elastic spring stiffness K_{sp} is determined using the cracked section properties of the shear wall. When the section at the base of walls attains its ultimate moment M_2, a flexural plastic hinge has been formed at the same location. The area moment of inertia of such a section after conversion of steel to concrete is called I_{cr} or the cracked section inertia.

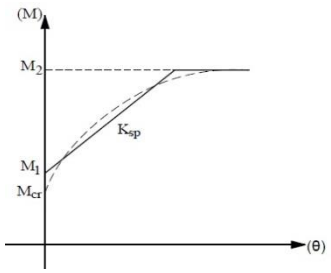

Figure 2. The macro model moment-rotation behavior at the base of a 3D shear wall

For a wall segment fixed at base having a moment of inertia I_{cr}, the relation between the bending moment at the base, M_p, and the relative rotation of the two ends, θ_p, is:

$$M_p = \frac{2E_c I_{cr}}{L_v}\theta_p + M_1 \quad (1)$$

Therefore:

$$K_{sp} = \frac{2E_c I_{cr}}{L_v} \quad (2)$$

where, L_v is the shear span being equal to moment-shear ratio at the wall base. I_{cr} is a function of section shape, configuration of the reinforcement and modulus of elasticity of steel and concrete.

For rectangular sections with concentrated reinforcement, I_{cr} can be easily computed using hand calculations. For 3D sections under study including H, T, and L sections with distributed longitudinal reinforcement, the same task is much more involved and deriving general formulas can be much helpful. This is done in this study as follows. The tensile zone of concrete is disregarded and strain and stress distributions in the compression zone are assumed to be linear. Area of steel is converted to an equivalent concrete area being *n*-times that of the steel with *n* being ratio of the elastic modulus of steel to that of the concrete. Then, position of the neutral axis is located using equilibrium and deformation compatibility relations. Finally, I_{cr} is calculated using the area of concrete in compression plus the converted tensile steel area.

An intensive parametric study was performed and some general formulas were derived for I_{cr} for the purposes of this study.

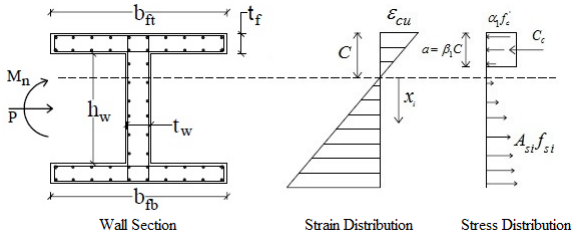

(I) Assume depth of neutral axis, C, and a=β_1C

(II) $\varepsilon_{si} = \varepsilon_{cu}\frac{C - x_i}{C}$, $f_y \geq f_{si} = E_s\varepsilon_{si} \geq -f_y$

(III) $C_C = \alpha_1 f_c' A_c$

(IV) If : $C_C + \sum A_{si} f_{si} = P$

Then:

$$M_2 = M_n = C_c\left(C - a/2\right) + \sum A_{si} f_{si} x_i + P\left(h_w/2 + t_f - C\right)$$

Else: Repeat from Step (I)

Where: $\varepsilon_{cu} = 0.0038$, $\alpha_1 = 0.85$, $\beta_1 = 0.85$ [19]

Figure 3. Calculation procedure of the ultimate moment, M_2 (=M_n)

In all, 5040 sections were studied. The concrete strength was varied between 16 and 48 MPa and the yield strain of steel was fixed at 0.002. Section shapes being L, T and H were examined with dimensions exhibited in Table 1, including 12 groups of analysis including 9 wall groups with 3 unsymmetric walls being loaded in two perpendicular directions.

By regression, the following relations are derived for I_{cr} for H-shape, L &T-shapes with flange in tension, and L & T-shapes with flange in compression, respectively:

$$\frac{I_{cr}}{I_g} = 0.018\frac{E_s}{E_c} + 0.112\ln\left(\frac{A_w}{A_{ct}}\right) + 0.015\ln\left(\frac{A_g}{A_{ct}}\right) - 0.0034\rho_f - 0.10 \quad (3)$$

$$\frac{I_{cr}}{I_g} = 0.021\frac{E_s}{E_c} + 0.141\ln\left(\frac{A_w}{A_{ct}}\right) - 0.192\ln\left(\frac{A_g}{A_{ct}}\right) + 0.22\rho_f - 0.205 \quad (4)$$

$$\frac{I_{cr}}{I_g} = 0.019\frac{E_s}{E_c} + 0.073\ln\left(\frac{A_w}{A_{ct}}\right) + 0.328\ln\left(\frac{A_g}{A_{ct}}\right) - 0.1236\rho_f - 0.431 \quad (5)$$

where, E_s is modulus of elasticity of steel, A_w area of web, A_{ct} area of wall section in tension (≈ area of flange), and ρ_f steel percentage in flange.

For example, in Figure 4 comparison between the proposed equation of I_{cr} for H-shape walls and the exact value is shown. The accuracy is quite satisfying.

3. 3. 4. The Equivalent Yield Moment, M_1 As shown in Figure 7, M_1 is somewhat larger than M_{cr}. Like M_{cr}, M_1 is dependent on the axial force, section shape, distribution of the longitudinal reinforcement, aspect ratio of wall in height and section, and mechanical properties of materials.

To calculate M_1, lateral displacement of the cantilever wall, Δ_w, under a horizontal load *F* applied at the height H_w, is calculated using the macro model of wall as:

$$\Delta_w = \Delta_{\text{elastic}} + \theta_p H_w \rightarrow \Delta_w = \frac{FH_w^{\,3}}{3E_c I_g} + \frac{M_2 - M_1}{K_{sp}}H_w \quad (6)$$

Equation (6) owes its simple shape to the macro model proposed. Therefore, using the fiber model, a lateral load is applied to the cantilever wall to produce a lateral displacement at the same place. It is increased up to the point where the longitudinal rebars yield and the lateral stiffness becomes just zero. For the walls under study, this happens at a drift of about 1%. Now, the base moment is M_2, the lateral load is *F*, and the lateral displacement is Δ_w. Then Equation (6) is used to determine M_1.

It is well known that M_{cr} is calculated using Equation (7):

$$M_{cr} = \frac{P}{A_g}S + f_{cr}S \quad (7)$$

where, *S* is the section modulus.

TABLE 2. Properties of the shear walls under study for determining I_{cr}

Shape	Code name	Height (m)	ρ(%)	b_f (mm)	t_f (mm)	h_w (mm)	t_w (mm)
A	BS1-ii	15	0.8, 1.5, 2	640-6400	300	5700	300
		21	0.8, 1.5, 2	640-6400	350	5650	350
		30	0.8, 1.5, 2	640-6400	400	5600	400
	BS1-i	15	0.8, 1.5, 2	640-6400	300	5700	300
		21	0.8, 1.5, 2	640-6400	300	5700	300
		30	0.8, 1.5, 2	640-6400	300	5700	300
		15	0.8, 1.5, 2	640-6400	300	2700	300
		21	0.8, 1.5, 2	640-6400	350	2650	350
		30	0.8, 1.5, 2	640-6400	400	2600	400
		15	0.8, 1.5, 2	640-6400	300	2700	300
		21	0.8, 1.5, 2	640-6400	300	2700	300
		30	0.8, 1.5, 2	640-6400	300	2700	300
B	BS2	15	0.8, 1.5, 2	680-5100	300	3400	300
		21	0.8, 1.5, 2	680-5100	350	3400	350
		30	0.8, 1.5, 2	680-5100	400	3400	400
C	BS3	15	0.8, 1.5, 2	640-6400	300	2850	300
		21	0.8, 1.5, 2	640-6400	350	2825	350
		30	0.8, 1.5, 2	640-6400	400	2800	400
	BS3-i	15	0.8, 1.5, 2	640-6400	300	5850	300
		21	0.8, 1.5, 2	640-6400	350	5825	350
		30	0.8, 1.5, 2	640-6400	400	5800	400
D	BS4	15	0.8, 1.5, 2	1000	400	5200	400
		21	0.8, 1.5, 2	1000	450	5100	450
		30	0.8, 1.5, 2	1000	500	5000	500

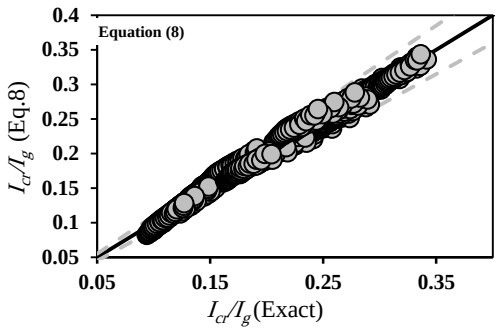

Figure 4. The approximate I_{cr} versus the exact values.

Then, M_1 can be calculated by a revision of Equation (7) as:

$$M_1 = \alpha \frac{P}{A_g} S + \beta f_{cr} S \quad (8)$$

Equation (8) shows that α is a factor for the effect of axial force and β for the tensile strength of concrete. Values of α and β, as calibration factors, depend on the same parameters that M_1 is a function of. Then, the following items are taken into account in the parametric studies to derive regression equations for α and β: The aspect ratio of wall, percentage of the longitudinal reinforcement, the axial force on the wall, and the wall's section shape. The strength of concrete is 24 MPa, yield strength of the rebars is 400 MPa, the axial force ratio P/f'_cA_g takes up the values 0.05, 0.10 and 0.15, reinforcement ratio in the tensile flange varies between 0.8-2% and height-length ratio of walls varies between 2.3 and 9.3. The section shapes are L, T, I and H, and the analysis includes 12 groups of walls each one including 9 wall samples with the three unsymmetric walls being loaded in two perpendicular directions separately.

To calculate α, it is easier to ignore the tensile strength of concrete first. Then the second term on the right side of Equation (5), including β, is eliminated and only α remains. Under a constant axial force of $0.05f'_cA_g$, 108 samples of walls are analyzed to calculate M_1 as described based on Equation (3) and then α from Equation (5). Then, 99 wall samples were analyzed first under an axial force of $0.10f'_cA_g$ and then $0.15f'_cA_g$ to evaluate effect of the axial force on α.

Thus, the total number of wall cases for determination of α is 306. Next, the condition of f_{cr} being zero is waived and Equation (5) is solved again for the same values of α to calculate β. This makes number of wall samples analyzed sum up to more than 450. The results are shown in Figure 5.

As for effect of the wall's aspect ratio, H/l_w with H being height and l_w length of wall, the parametric study shows that α varies almost linearly with this parameter while β remains almost unchanged with H/l_w.

Variation of the percentage of the tensile reinforcement in the concrete tensile area, ρ, changes α up to 30%. Again, this variation tends to be linear. This is expected, because increase of ρ results in a larger bending capacity of the section, while M_{cr} remains almost unchanged. Effect of ρ on α is stronger than H/l_w. Again it has almost no effect on β.

The section shape can be quantified using the ratios A_w/A_{ct} and A_g/A_{ct} where A_{ct} is area of the tensile flange (in rectangular sections area of the boundary element), and A_w the area of the web.

It is seen that β changes with the section shape contrary to other factors where β did not change. Based on the above discussion, α is taken to change linearly with the aspect ratio, section shape and reinforcement ratio, and to have a second order relation with the axial force ratio. β is assumed to vary only with the section shape. Then:

$$\alpha = \left[1.53 + 0.08\left(\frac{H}{l_w}\right) + 0.38\left(\frac{A_w}{A_{ct}}\right) - 0.15\left(\frac{A_g}{A_{ct}}\right) + 0.32\rho_f\right] \times \left[26\left(\frac{P}{f_c' A_g}\right)^2 - 8.35\left(\frac{P}{f_c' A_g}\right) + 1.35\right] \quad (9)$$

The section shape can be quantified using the ratios A_w/A_{ct} and A_g/A_{ct} where A_{ct} is area of the tensile flange (in rectangular sections area of the boundary element), and A_w the area of the web.

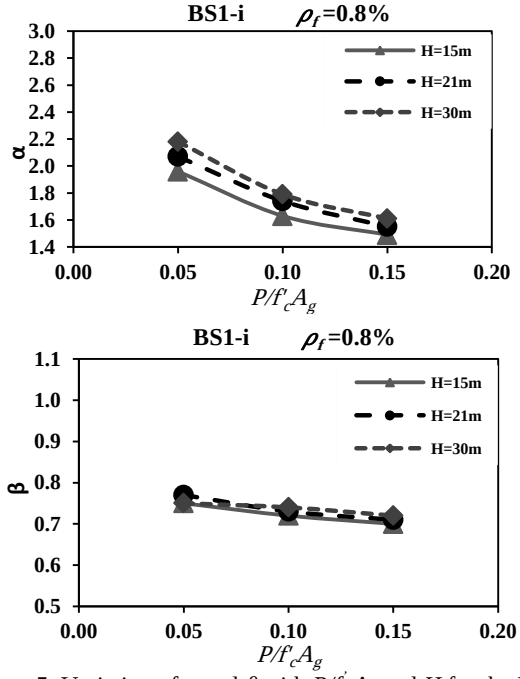

Figure 5. Variation of α and β with $P/f_c'A_g$ and H for the BS1-i wall

It is seen that β changes with the section shape contrary to other factors where β did not change. Based on the above discussion, α is taken to change linearly with the aspect ratio, section shape and reinforcement ratio, and to have a second order relation with the axial force ratio. β is assumed to vary only with the section shape. Then:

$$\alpha = \left[1.53 + 0.08\left(\frac{H}{l_w}\right) + 0.38\left(\frac{A_w}{A_{ct}}\right) - 0.15\left(\frac{A_g}{A_{ct}}\right) + 0.32\rho_f\right] \times \left[26\left(\frac{P}{f_c' A_g}\right)^2 - 8.35\left(\frac{P}{f_c' A_g}\right) + 1.35\right] \quad (9)$$

$$\beta = 0.10\left(\frac{A_w}{A_{ct}}\right) - 0.005\left(\frac{A_g}{A_{ct}}\right) + 0.70 \quad (10)$$

Here, A_{ct} and ρ_f are area of the tensile flange and percentage of the tensile rebars of A_{ct}. In rectangular walls, these parameters refer to the concrete area and rebar percentage of the tensile boundary element.

3. 4. Numerical Evaluation Accuracy of the developed macro model in producing the moment-rotation path is evaluated using Equations (1)-(8) in comparison to the meso model and the code procedure. Since values of the factors of equations for K_{sp} and M_1 were calculated based on the same walls with regression, this section is meant only to evaluate scattering of the macro model results with regard to the more precise values of the meso model. The parameters considered in the macro model of ASCE41-13 include confinement of the boundary member of the shear wall, ultimate compressive strength of concrete, yield strength and area of the longitudinal rebars, axial load ratio, thickness and length of the shear wall, and magnitude of the shear force in the wall. Linear behavior of the RC wall before cracking is not considered in the code's model for the walls controlled by flexure. Figure 6 shows the force-displacement curves of the studied walls calculated with different methods. The excellent accuracy of the proposed macro model is evident. This is while the code-based prescribed method is in large error in many cases.

4. CONCLUSIONS

In this paper a general macro model for nonlinear moment-rotation behavior of 3D RC shear walls was developed for monotonic loading cases. Shear walls being H, L, and T in cross-section shape were considered. A detailed nonlinear finite element model of the selected walls was first established based on results of experiments on certain 3D walls.

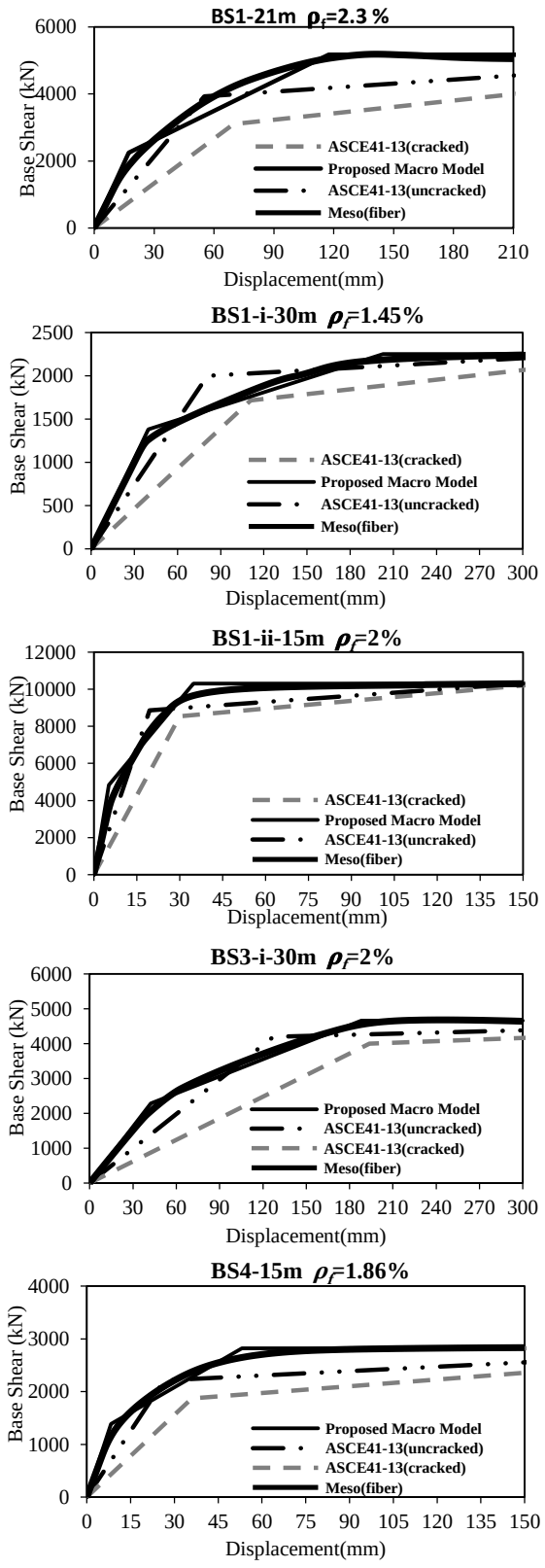

Figure 6. The force-displacement curves of the studied 3D shear walls calculated with different methods

Because of heavy involvement of such a model, a substitute fiber-element model was also developed and calibrated for all of the cases studied in this research with regard to the finite element models. Then, a simple tri-linear macro model, substituting the nonlinear wall with a linear one resting on a concentrated rotational spring at base was developed. Characteristics of the model were calculated using analytical equations that contained numerical factors calculated by regression between 450 wall cases. Suitability and superior accuracy of the model were shown through a large number of numerical examples of 3D walls.

The developed three-parameter macro model is both accurate and fast for the common range of geometrical dimensions and mechanical properties of 3D shear walls. On the other hand, it is appropriate only for the walls governed by flexural deformations and for when the global behavior of wall is meant to be evaluated. Although it is derived for monotonic loading, its extension to cyclic loads can be accomplished with a similar procedure.

5. REFERENCES

1. Engineers, A.S.o.C. and Institute, S.E., "Seismic evaluation and retrofit of existing buildings, American Society of Civil Engineers., (2014).
2. Zhang, P., Li, Q. and Li, X., "Experimental research on seismic performance of short pier shear wall with l-shaped section [j]", ***Journal of Earthquake Engineering and Engineering Vibration***, Vol. 4, No., (2010), 51-56.
3. Zhang, J. and Lu, Z., "Earthquake simulation test of short leg shear wall tube model", ***Journal of Southeast University***, Vol. 31, No. 6, (2001), 4-8.
4. Taylor, C.P., Cote, P.A. and Wallace, J.W., "Design of slender reinforced concrete walls with openings", ***Structural Journal***, Vol. 95, No. 4, (1998), 420-433.
5. Thomsen IV, J.H. and Wallace, J.W., "Displacement-based design of slender reinforced concrete structural walls—experimental verification", ***Journal of Structural Engineering***, Vol. 130, No. 4, (2004), 618-630.
6. Chen, Z., Xu, J., Chen, Y. and Su, Y., "Seismic behavior of t-shaped steel reinforced high strength concrete short-limb shear walls under low cyclic reversed loading", ***Structural Engineering and Mechanics***, Vol. 57, No. 4, (2016), 681-701.
7. Wang, X., Su, Y. and Yan, L., "Experimental and numerical study on steel reinforced high-strength concrete short-leg shear walls", ***Journal of Constructional Steel Research***, Vol. 101, (2014), 242-253.
8. Valoroso, N., Marmo, F. and Sessa, S., "Limit state analysis of reinforced shear walls", ***Engineering Structures***, Vol. 61, (2014), 127-139.
9. Mousavi, S.A., Zahrai, S.M. and Bahrami-Rad, A., "Quasi-static cyclic tests on super-lightweight eps concrete shear walls", ***Engineering Structures***, Vol. 65, (2014), 62-75.
10. Pugh, J.S., Lowes, L.N. and Lehman, D.E., "Nonlinear line-element modeling of flexural reinforced concrete walls", ***Engineering Structures***, Vol. 104, (2015), 174-192.

11. Ergun, M. and Ates, S., "The stress analysis of a shear wall with matrix displacement method", ***Structural Engineering and Mechanics***, Vol. 53, No. 2, (2015), 205-226.
12. Lestuzzi, P. and Badoux, M., "The γ-model: A simple hysteretic model for reinforced concrete walls", in Proceedings of the fib-Symposium., (2003).
13. Parulekar, Y., Reddy, G., Singh, R., Gopalkrishnan, N. and Ramarao, G., "Seismic performance evaluation of mid-rise shear walls: Experiments and analysis", ***Structural Engineering and Mechanics***, Vol. 59, No. 2, (2016), 291-312.
14. MULAS, M.G., "Shaking table tests on rc shear walls: Significance of numerical modeling", POLITECNICO DI MILANO, (2007),
15. Kim, T. and Foutch, D.A., "Application of fema methodology to rc shear wall buildings governed by flexure", ***Engineering Structures***, Vol. 29, No. 10, (2007), 2514-2522.
16. Linde, P. and Bachmann, H., "Dynamic modelling and design of earthquake-resistant walls", ***Earthquake Engineering &Structural Dynamics***, Vol. 23, No. 12, (1994), 1331-1350.
17. Li, G., Zhang, F., Zhang, Y. and Li, H.N., "Nonlinear hysteretic behavior simulation of reinforced concrete shear walls using the force analogy method", ***The Structural Design of Tall and Special Buildings***, Vol. 24, No. 7, (2015), 504-520.
18. ABAQUS, C., *Analysis user's manual, version 6.12*. 2012, ABAQUS.
19. 318, A.C., "Building code requirements for structural concrete (ACI 318-11M) and commentary, American Concrete Institute., (2011).
20. Basu, P.C., Shyiamoni, P. and Roshan, A., "Characterisation of steel reinforcement for rc structures: An overview and related issues", ***Indian Concrete Journal***, Vol. 78, No. 1, (2004), 19-30.
21. Mazzoni, S., McKenna, F., Scott, M. and Fenves, G., "Opensees command language manual. Open system for earthquake engineering simulation (opensees), pacific earthquake engineering research (peer) center", ***University of California, Berkeley, California, USA***, (2006).
22. Adebar, P., Ibrahim, A.M. and Bryson, M., "Test of high-rise core wall: Effective stiffness for seismic analysis", ***ACI Structural Journal***, Vol. 104, No. 5, (2007), 549-559.

A Macro-model for Nonlinear Analysis of 3D Reinforced Concrete Shear Walls

M. Heydari, F. Behnamfar, H. Zibasokhan

Department of Civil Engineering, Isfahan University of Technology, Esfahan, Iran

P A P E R I N F O

Paper history:
Received 09 May 2016
Received in revised form 13 September 2017
Accepted 12 October 2017

Keywords:
Micro Model
Meso Model
Macro Model
Nonlinear Analysis
3D RC Shear Wall

چکیده

در این تحقیق، حدود ۴۵۰ نمونه دیوار برشی با شکل‌ها و ارتفاع‌های مختلف بررسی شده است. این نمونه‌ها شامل دیوار برشی های L، T و H شکل، هستندکه با استفاده از مدل میکرو در نرم افزار آباکوس با استفاده از مدل‌سازی و تحلیل به روش اجزاء محدود به صورت غیرخطی بررسی شده‌اند. همچنین، مدل‌سازی مزو با استفاده از المان‌های فیبری در نرم‌افزار اوپن‌سیس انجام شده است. این تحقیق نشان داد که مدل مزو در عین داشتن دقت مناسب از سرعت بسیار بیشتری نسبت به مدل میکرو برخوردار است. در ادامه، یک ماکرو مدل خمشی دارای رفتار غیرخطی با استفاده از فنر دورانی متمرکز در پایین دیوار پیشنهاد شده است. نیروی محوری، شکل مقطع دیوار، درصد آرماتورهای طولی و نسبت شکل دیوار به عنوان عوامل اصلی اثر گذار بر رفتار دیوار در تعیین مشخصات این فنر دورانی مورد استفاده قرار گرفته است. برای تعیین سریع منحنی لنگر-دوران فنر دورانی، با استفاده از برازش روابط نیمه تحلیلی پیشنهاد شده است. مقایسه نتایج ماکرو مدل توسعه داده شده با نتایج مدل میکرو و نتایج آزمایشگاهی موجود نشان دهنده دقت مناسب این مدل است.

***doi**: 10.5829/ije.2018.31.02b.05*